ACS SyntheticBiology

pubs.acs.org/synthbio

Technical Note

Designing Single-Component Optogenetic Membrane Recruitment Systems: The Rho-Family GTPase Signaling Toolbox

Erin E. Berlew, Keisuke Yamada, Ivan A. Kuznetsov, Eleanor A. Rand, Chandler C. Ochs, Zaynab Jaber, Kevin H. Gardner, and Brian Y. Chow*

Cite This: *ACS Synth. Biol.* 2022, 11, 515–521

Read Online

ACCESS | Metrics & More | Article Recommendations | Supporting Information

ABSTRACT: We describe the efficient creation of single-component optogenetic tools for membrane recruitment-based signaling perturbation using BcLOV4 technology. The workflow requires two plasmids to create six different domain arrangements of the dynamic membrane binder BcLOV4, a fluorescent reporter, and the fused signaling protein of interest. Screening of this limited set of genetic constructs for expression characteristics and dynamic translocation in response to one pulse of light is sufficient to identify viable signaling control tools. The reliability of this streamlined approach is demonstrated by the creation of an optogenetic Cdc42 GTPase and Rac1-activating Tiam1 GEF protein, which together with our other recently reported technologies, completes a toolbox for spatiotemporally precise induction of Rho-family GTPase signaling at the GEF or GTPase level, for driving filopodial protrusions, lamellipodial protrusions, and cell contractility, respectively mediated by Cdc42, Rac1, and RhoA.

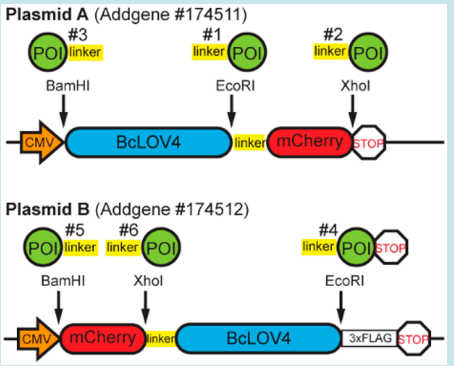

KEYWORDS: *optogenetics, BcLOV4, Rho GTPase, Cdc42, Tiam1*

INTRODUCTION

Signaling at the plasma membrane governs how cells sense, respond to, and interact with their external chemical and mechanical environments. The signaling events are largely mediated by diverse protein−protein interactions (PPI) and protein−lipid interactions (PLI) at the inner leaflet that initiate downstream cascades in the cytoskeleton and cytoplasm. Since modest changes in the local concentration and/or enzymatic activity of peripheral membrane proteins can have profound effects throughout the cell, their regulation must be tight in space and time, and the study of this coordination is critical to understanding cellular dynamics.

Signaling induction by optogenetic membrane recruitment allows these regulatory dynamics to be interrogated by a spatiotemporally precise perturbation. Initially reported using an engineered chimera of the AsLOV2 photosensory domain[1,2] fused to a phospholipid binding domain (of RIT GTPase),[3] "single-component" recruitment by direct association with the inner leaflet, without a heterodimerization partner, offers experimental simplicity in that it requires only one transgene (to be delivered, expressed, and visualized). The endogenous binding partner is in natural excess at the membrane to avoid binding-site availability limitations that reduce signaling fold-change and compromise spatiotemporal resolution by increasing diffusional length/time before stable association.[3−8]

BcLOV4,[9,10] is a photoreceptor from *Botrytis cinerea* that, as we previously showed, directly binds plasma membrane lipids following blue light stimulus via an amphipathic helix-mediated electrostatic interaction (Figure 1a). It is a natural single-component system whose rapid membrane association/dissociation kinetics (τ_{on} ∼ seconds and τ_{off} ∼ 1 min) and slow lateral diffusion (D_{mem} < 0.028 $\mu m^2/s$) are favorable to high performance control. It is a versatile technology with which we have engineered numerous chimeric Rho-family GTPases and GEF proteins created by a common workflow that involved six engineered genetic constructs.[6−8]

In this technical report, we describe a streamlined workflow with improvements in yield and throughput to facilitate the creation of BcLOV4-based optogenetic tools by others. The system uses two plasmids to create the six domain arrangements that permute BcLOV4, mCherry fluorescent reporter, and the fusion protein of interest (POI). Also of note, a peptidyl cap has been added that promotes the folding of genetic constructs with BcLOV4 as the C-terminal domain, two arrangements that were previously disfavored[7,8] in our previous engineering efforts, thereby recovering their applicability. We used this workflow to create two new tools (opto-Cdc42 and opto-Tiam1) to complete the BcLOV4-derived single-component toolbox for activating Rho-family GTPase

Received: December 3, 2021
Published: January 3, 2022

https://doi.org/10.1021/acssynbio.1c00604
ACS Synth. Biol. 2022, 11, 515−521

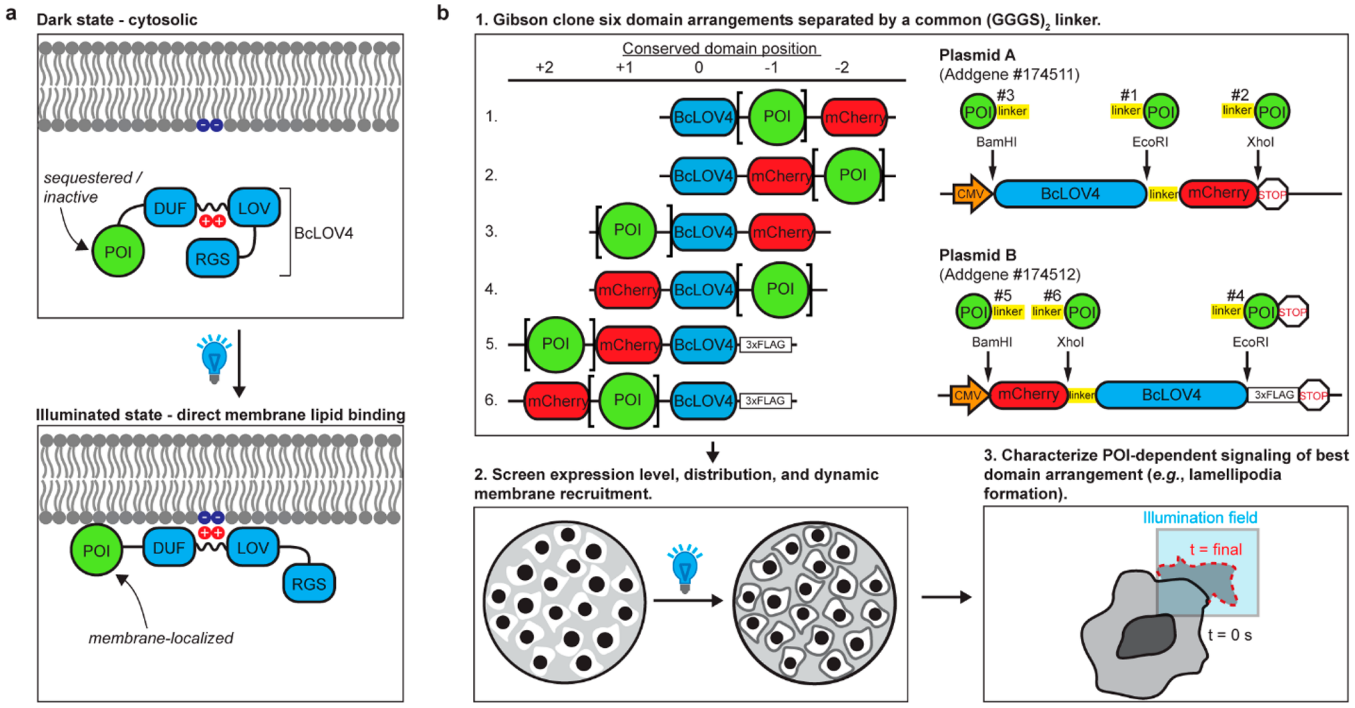

Figure 1. Engineering workflow for creating single-component BcLOV4-derived optogenetic tools. (a) Schematic of BcLOV4-mediated protein-of-interest (POI) recruitment to the plasma membrane via direct binding of the BcLOV4 amphipathic helix to inner-leaflet phospholipid head groups. LOV = light-oxygen-voltage domain. DUF = domain of unidentified function. RGS = regulator of G-protein signaling domain (inert in mammalian and yeast cells). (b) Molecular cloning and screening scheme. Six domain arrangements are cloned using a two-plasmid set, with predefined insertion sites for Gibson cloning that are $(GGGS)_2$ linkers of different codon usage. Expression characteristics and dynamic membrane recruitment are sufficient screening parameters to identify functional POI fusions.

signaling, spanning the GTPases and their respectively selective GEF activators for inducing filopodia (Cdc42 and Intersectin-1), lamellipodia (Rac1 and Tiam1), and contractile constrictions and blebs (RhoA and ARHGEF11), for studying important cytoskeletal processes such as migration, cytokinesis, and axon elongation.

RESULTS AND DISCUSSION

Molecular Engineering Workflow. The six positional arrangements of BcLOV4, mCherry, and the POI (separated by flexible $(GGGS)_2$ linkers) are created in a mammalian backbone and then tested in transfected HEK293T cells (Figure 1b). The transgene is under a ubiquitous CMV promoter in the pcDNA3.1 backbone. In the new simplified strategy, only two (not six) plasmids with predefined POI-insertion sites are needed to generate all the arrangements in-frame by Gibson cloning (see Supporting Information). The initial screening stage identifies constructs of high cytosolic expression that is generally homogeneous across the population and of uniform and nonpunctate subcellular distribution in the dark-adapted state, as measured in live cells by fluorescence microscopy. Robust membrane translocation induced by a single 5 s-long blue-light pulse (saturating ≥15 mW/cm^2 @ λ = 450 nm) is then assayed before characterizing any specific POI-mediated pathway activation. Note that the apparent increase in membrane-bound protein fluorescence following blue light stimulation will vary by microscope due to diffractive effects; as an estimate for a 63× magnification objective, BcLOV4 shows a 1.308 ± 0.048 membrane-to-cytosol fluorescence ratio on a widefield or epifluorescence microscope, corresponding to a 6.613 ± 1.25 ratio observed on a confocal microscope (mean ± std. error, N = 20 cells) across the instruments in our previous reports.[7,8,10] Across the six BcLOV4 fusions to be described here, the translocation assay is reasonably predictive of an eventual inducible signaling function by the POI.

In addition to simplifying the cloning, plasmid B of the two-plasmid set contains a C-terminal 3x-FLAG epitope as a peptidyl cap to improve folding. Previously, we observed that constructs with BcLOV4 at the C-terminus were consistently disfavored, where the expression appeared lit-like in the dark-adapted state with protein localized to the membrane and aggregated on lysosomes throughout the cytosol. However, the addition of the peptidyl cap (GGGS-3xFLAG) recovered the normal expression pattern without disrupting its reversible membrane translocation (Supplementary Figures 1 and 2). Attempts to recover the cytosolic expression of dark-adapted BcLOV4 via mutagenesis of its hydrophobic C-terminal phenylalanine residue were unsuccessful (Supplementary Figure 3). This disfavored phenotype also held for tool screening domain arrangements with BcLOV4 at the C-terminus of the protein, regardless of POI domain type or signaling pathway, suggesting that the combination of protein bulk at the N-terminus and an exposed BcLOV4 C-terminus results in aberrant lipid-binding amphipathic helix exposure in the dark (Supplementary Figure 4). This capping strategy is generally applicable, successfully rescuing the normal dark-state expression of otherwise disfavored domain arrangements for previously reported effectors Intersectin1 (Cdc42-GEF), Rac1 GTPase, RhoA GTPase, and ARHGEF11 (RhoA-GEF) (Supplementary Figure 5).

Toolbox for Rho-Family GTPase Signaling Activation. We used this improved workflow to create optogenetic Cdc42

https://doi.org/10.1021/acssynbio.1c00604
ACS Synth. Biol. 2022, 11, 515−521

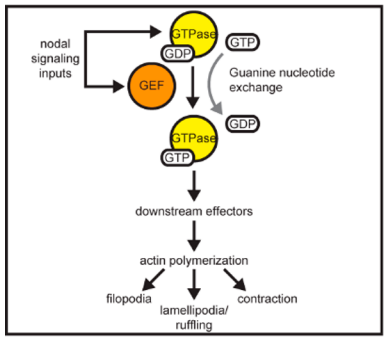

b

TOOL/ ADDGENE #	PATHWAY	DOMAIN ARRANGEMENT	PHENOTYPE	REFERENCE (PMID)
opto-Cdc42 174510	Cdc42	mCherry-Cdc42-BcLOV4-3xFLAG	Filopodia	*this work*
opto-Itsn1 174509	Cdc42 GEF	Itsn1-BcLOV4-mCherry	Filopodia	30884362
opto-Rac1 135396	Rac1	BcLOV4-Rac1-mCherry	Lamellipodia	32048687
opto-Tiam1 174508	Rac1 GEF	BcLOV4-Tiam1-mCherry	Lamellipodia (serum starved) Ruffling/lamellipodia (serum fed)	*this work*
opto-RhoA 164472	RhoA	RhoA-BcLOV4-mCherry	Stress fibers	34288599
opto-RhoGEF 164473	RhoA GEF	BcLOV4-RhoGEF-mCherry	Stress fibers	34288599

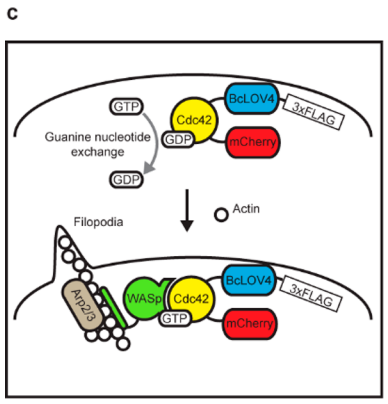

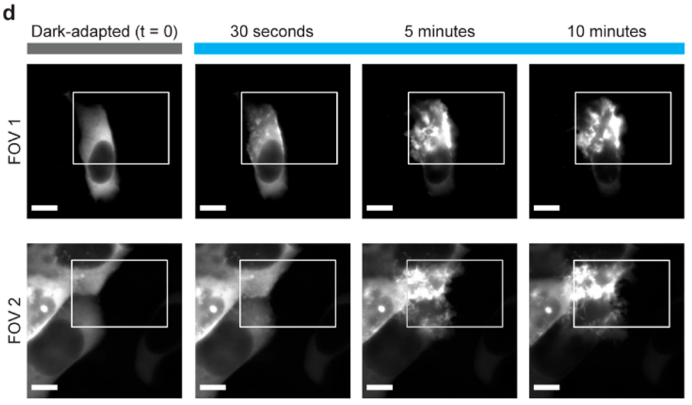

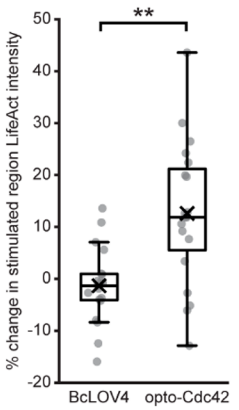

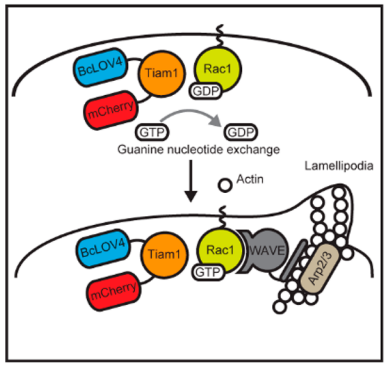

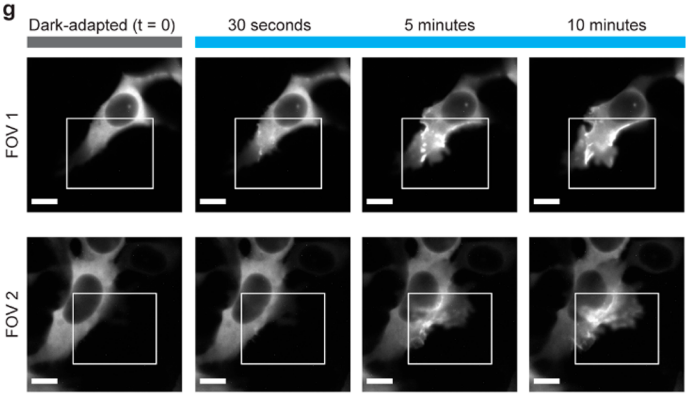

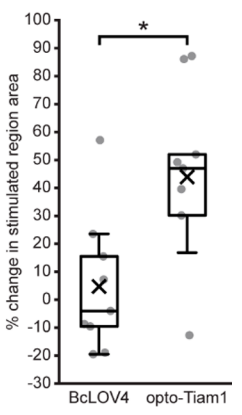

Figure 2. BcLOV4 toolbox for Rho-family GTPase signaling activation. (a) Nodal activation of Rho-family signaling and actin polymerization by GTPases and GEFs. (b) Summary of BcLOV4-derived tools for enhanced signaling of Cdc42, Rac1, and RhoA initiated at the GEF and GTPase level. (c) Schematized induction of filopodia formation by opto-Cdc42 activation. (d) Exemplar images of opto-Cdc42-induced filopodia formation with pulsatile patterned stimulation (1.6% duty ratio), visualized by mCherry fluorescence. White box = blue-light illumination field. Scale = 10 μm. (e) Percent change in miRFP703-LifeAct fluorescence intensity within the stimulated region, compared to BcLOV4-mCherry control. Center line, median; "X", mean; box limits, upper and lower quartiles; whiskers, 1.5× interquartile ranges. Mann−Whitney U test, uncorrected for multiple comparisons. (**) = $p < 0.01$. $d > 0.5$. $N = 18$ independent videos per condition. (f) Schematized induction of lamellipodia formation by opto-Tiam1 activation. (g) Exemplar images of opto-Tiam1-induced lamellipodia formation with pulsatile patterned stimulation (1.6% duty ratio), visualized by mCherry fluorescence. White box = illumination field. Scale = 10 μm. (h) Percent change cell area within the stimulated region, compared to BcLOV4-mCherry control. Center line, median; "X", mean; box limits, upper and lower quartiles; whiskers, 1.5× interquartile ranges. Mann−Whitney U test, uncorrected for multiple comparisons. (*) = $p < 0.05$. $d > 0.5$. $N = 9$ independent videos per condition.

GTPase and Rac1 GEF Tiam1 (Figure 2a,b). The Rho family of small GTPases are molecular switches that regulate cytoskeletal dynamics by initiating signaling cascades resulting in actin reorganization.[11−13] The GTPases are activated through GTP loading by guanine nucleotide exchange factors (GEFs).[14,15] Members of this family have been engineered primarily by optogenetic heterodimerization, but also by photoswitching and photo-oligomerization, as summarized in Supplementary Table 1 (and references therein). We here sought to add to existing BcLOV4-derived tools to initiate signaling at the GEF- or GTPase-level for the three most-studied proteins (Cdc42, Rac1, and RhoA), together comprising a comprehensive toolbox for Rho-family signaling activation on the same photoreceptor platform.

The genetic construct mCherry-Cdc42-BcLOV4-3xFLAG was designated as opto-Cdc42 (Figure 2c and Supplementary

https://doi.org/10.1021/acssynbio.1c00604
ACS Synth. Biol. 2022, 11, 515−521

Figures 6−7). We used wildtype or GDP-bound Cdc42 GTPase in constructing this tool, to be consistent with our previously reported Rac1[7] and RhoA[8] GTPase tools. Previous work by others demonstrated that the membrane localization of Cdc42[16,17] corecruits its GEF and is thus sufficient for pathway induction, which is in agreement with single-molecule imaging studies of Rho-family GTPases.[18] Blue light stimulation of opto-Cdc42-expressing HEK cells resulted in selective protein recruitment to the plasma membrane within an optically patterned stimulation region and consequent formation of finger-like projections (Figure 2d). To quantify these filopodia, cotransfected LifeAct-miRFP703 was visualized for filamentous actin polymerization extent in response to modest pulsatile stimulation (1.6% duty cycle over 10 min). The change in LifeAct fluorescence intensity in the stimulated region, normalized to the nonstimulated region of the cell, was significantly statistically different and of large effect size in opto-Cdc42 cells vs BcLOV4-mCherry negative control (Figure 2e). The filopodia formation was abrogated by pharmacological inhibition of its interactions with endogenous GEFs (by ZCL-278 treatment) or by inhibition of actin-related protein 2/3 (Arp2/3) activity (by CK-666 treatment), thus indicating that opto-Cdc42 is initially GDP-bound in the dark-adapted state and that its induction of cytoskeletal signaling is dependent on canonical regulatory pathways (Supplementary Figure 7). Opto-Cdc42 and previously reported Cdc42-GEF opto-Itsn1 (which we previously called opto-DHPH[6]) provide two nodes of control of cellular Cdc42 signaling using the BcLOV4 platform.

The genetic construct BcLOV4-Tiam1-mCherry was designated as opto-Tiam1 (Figure 2f and Supplementary Figures 8−9). Upon membrane recruitment, opto-Tiam1 drove sheet-like lamellipodia formation (Figure 2g) as quantified by the change in cell area within the optically stimulated region, which significantly increased statistically, and by a large effect size in opto-Tiam1 expressing cells vs BcLOV4-mCherry control (Figure 2h). Pharmacological inhibition of Rac1::-Tiam1 interactions (by NSC-23766 treatment) or inhibition of Arp2/3 each suppressed lamellipodia formation, indicating that the induced cytoskeletal changes involved the endogenous pool of Rac1 GTPase and were also dependent on canonical regulatory pathways.

It is worth noting that the opto-Tiam1 analysis was performed with serum-starved cells. When assessing opto-Tiam1 activity in serum-fed cells, membrane ruffles and/or lamellipodia formed within the stimulated region (Supplementary Figure 8f). While membrane ruffling is known to be dependent on Tiam1- and Rac1-dependent signaling,[19−21] consistent sheet-like projections were expected as the predominant cytoskeletal response, as was the case with opto-Rac1 under all conditions. Others have reported that dynamic membrane recruitment of Tiam1 with the optogenetic heterodimerizer iLID preferentially induces membrane ruffles[4] and filopodia,[22] without resolution of the inconsistency. It is known, though, that low cytoskeletal tension and focal adhesion strength in serum-starved cells result in easier cytoskeletal remodeling[23,24] that is permissive of lamellipodial persistence, and that under conditions of poor lamellipodial persistence, ruffling will instead occur.[25] Indeed, serum-starvation of opto-Tiam1 cells for 24 h prior to imaging resulted in consistent formation of lamellipodial sheets (Figure 2g and Supplementary Figure 8g). Opto-Tiam1 complements our previously published opto-Rac1 for GEF-level activation of the Rac1 signaling pathway. The association and dissociation time constants for opto-Cdc42 and opto-Tiam1 were similar to those for BcLOV4-mCherry control (Supplementary Figure 10).

In this work, we have described a streamlined approach for engineering single-component tools with BcLOV4 optogenetic technology to control cell signaling by dynamic membrane recruitment. We have applied it to complete a toolbox for inducible cytoskeletal control via activated signaling of the major Rho-family GTPases, all with one common optogenetic platform. The spatiotemporal resolution of these BcLOV4-based tools is anticipated to be generally favorable to existing optogenetic Rho-family tools, owing to rapid membrane interaction kinetics and submobile lateral diffusion of BcLOV4 that together determine characteristic membrane diffusional lengths.[4,26,27] Additionally, the excess binding site availability along the sink-like endogenous inner leaflet may minimize cytosolic-diffusional resolution loss known to be critical in optogenetic heterodimerization when binding site-limited[4] (*i.e.*, common stoichiometric expression conditions). However, as other approaches have been utilized to great effect to study Rho-family GTPase signaling, the benefit of the toolbox described herein lies in its completeness and experimental simplicity. The use of one common platform limits the technology-specific experimental optimization needed, and simple single-component approaches require minimal genetic payload, metabolic load, and/or consumption of optical bandwidth otherwise useful for reporter imaging. These features make the toolbox particularly useful for the nodal dissection of spatiotemporal dynamics and feedback in cell motility[28,29] and the study of how signals are integrated across the extensive interaction networks of these GTPase signaling pathways.[30]

It is worth noting that the best performing domain arrangement varied across the Rho-family toolbox (Figure 2b), including fusions (of the fluorescent reporter, GEF, or GTPase) to the N- or C-terminus of the wildtype BcLOV4 protein. Thus, BcLOV4 tolerates different domain arrangements and is not constrained to a "one-size-fits-all" architecture for success. The viability of two previously disfavored domain arrangements (with BcLOV4 as the C-terminal end of the total fusion construct), which was rescued by incorporating a C-terminal peptidyl cap, was particularly important here in creating opto-Cdc42 which relies on such an arrangement. The engineering workflow is likely to successfully yield high-performance tools for other POIs, as no other engineering optimization or strategy was required to create any of the tools described herein. The flexibility of the BcLOV4 platform and efficiency with which chimeras can be successfully engineered will facilitate the creation of other single-component membrane recruitment tools with other diverse POIs. The two-plasmid set is available on Addgene (plasmids 174511 and 174512), along with the Rho-family activation toolbox (see Figure 2b for plasmid numbers) [*Author note*: To be released upon publication].

MATERIALS AND METHODS

Genetic Constructs. Domain arrangement combinations of BcLOV4, mCherry, and proteins-of-interest (with a flexible $(GGGS)_2$ linker between each pair) were assembled by Gibson cloning using NEB HiFi DNA Assembly Master Mix (E2621) into the pcDNA3.1 mammalian expression vector under the CMV promoter. BcLOV4 and mCherry were amplified from

https://doi.org/10.1021/acssynbio.1c00604
ACS Synth. Biol. 2022, 11, 515−521

their mammalian codon-optimized reported fusion (Addgene plasmid 114595).[10] Wildtype Cdc42 GTPase was amplified from CLPIT Cry2PHR-mCherry-Cdc42, a kind gift from Dr. Lukasz Bugaj, with the "CAAX" removed to prevent prenylation. The DH domain of Tiam1 was identified using the PROSITE ExPASy database and amplified from pMXs3-TIAM1 (Addgene plasmid 86143). Other effectors were amplified from previously reported plasmids, all available on Addgene: Rac1 (plasmid 135396),[7] Intersectin1-DHPH (plasmid 174509),[6] RhoA (plasmid 164472), ARHGEF11-DH (plasmid 164473).[31] Genetic constructs were transformed into competent *E. coli* (New England Biolabs, C2984H), and sequence-verified by Sanger sequencing. For filopodia quantification, the miRFP703-tagged LifeAct plasmid was acquired from Addgene (plasmid 79993). Plasmids for opto-Tiam1 and opto-Cdc42 (plasmids 174508 and 174509) and plasmids for POI screening of BcLOV4 fusions (plasmids 174511 and 174512) will be available through Addgene.

Mammalian Culture and Transduction. HEK293T (ATCC, CRL-3216) cells were cultured in D10 media composed of Dulbecco's Modified Eagle Medium with Glutamax (Invitrogen, 10566016), supplemented with 10% heat-inactivated fetal bovine serum (FBS) and penicillin-streptomycin at 100 U mL^{-1}. Cells were maintained in a 5% CO_2 water-jacketed incubator (Thermo/Forma 3110) at 37 °C. Cells were seeded onto poly D-lysine-treated glass bottom dishes (MatTek, P35GC-1.5−14-C) at 15−20% confluency. Cells were transfected at ∼30−40% confluency 24 h later using the TransIT-293 transfection reagent (Mirus Bio, MIR2700) according to manufacturer instructions. Cells were imaged 24−48 h post-transfection. For experiments imaging actin polymerization, full media was replaced with serum starvation media (2% heat-inactivated FBS) at transfection.

Optical Hardware. Fluorescence microscopy was performed on an automated Leica DMI6000B fluorescence microscope under Leica MetaMorph control, with a sCMOS camera (pco.edge), an LED illuminator (Lumencor Spectra-X), and a 63× oil immersion objective. Excitation illumination was filtered at the LED source (mCherry imaging λ = 575/25 nm; GFP imaging or wide-field BcLOV4 stimulation λ = 470/24 nm; miRFP imaging λ = 632/22 nm). Fluorescent proteins were imaged with Chroma filters: mCherry (T585lpxr dichroic mirror, ET630/75 nm emission filter, 0.2−0.5 s exposure), GFP (T495lpxr dichroic mirror, ET 525/50 nm emission filter, 0.2 s exposure), miRFP703 (AT655dc dichroic mirror, ET655 nm emission filter, 0.5 s exposure). Cells were imaged at room temperature in CO_2-independent media (phenol-free HBSS supplemented with 1% L-glutamine, 1% penicillin−streptomycin, 2% essential amino acids, 1% nonessential amino acids, 2.5% HEPES pH 7.0, and 10% serum); LifeAct and lamellipodia imaging were performed in CO_2-independent media without serum. The spatially patterned illuminator was custom-constructed from a digital light processor (DLP, Digital Light Innovations CEL5500), as previously described.[7]

Expression Characterization and Membrane Translocation Assays. For membrane recruitment quantification, prenylated GFP was cotransfected as a membrane marker with the BcLOV4 fusions as previously described.[7,10,31] Briefly, an mCherry fluorescence image (500 ms exposure) was captured to assess protein expression level and subcellular distribution. Cells were then illuminated with a 5 s-long blue light pulse to stimulate BcLOV4, during which time mCherry fluorescence images were also captured every 200 ms to monitor subcellular localization changes. The GFP membrane marker was imaged immediately after blue light stimulation for correlation analysis. For membrane dissociation via thermal reversion of the photoactivated protein in the dark, mCherry was visualized every 5 s for 10−15 min in the absence of blue light stimulation. Membrane localization and dissociation were measured by line section analysis and correlation with prenylated GFP in ImageJ and MATLAB as previously described.[10]

Cytoskeletal and Morphological Dynamics. mCherry fluorescence was imaged every 15 s for 10 min. During this time, cells were stimulated for one second per minute (1.6% duty cycle) with spatially patterned illumination (25 μm-wide square encompassing ∼25% of cell area). For LifeAct imaging, miRFP fluorescence was imaged every 1 min.

Pharmacological Inhibitor Assays. Inhibitors were added to cells prior to imaging at the following concentrations and time points: Cdc42 inhibitor ZCL 278 (Cayman Chemical, 14849), 7.5 μM, 2 h prior to imaging; Rac1 GEF inhibitor NSC 23766 (Cayman Chemical, 13196), 50 μM, 24 h prior to imaging; Arp2/3 inhibitor CK-666 (Millipore-Sigma, SML0006), 500 μM, 6 h prior to imaging; actin polymerization inhibitor cytochalasin D (Cayman Chemical, 11330), 10 μM, 1 h prior to imaging.

Lateral Diffusion Measurements. FRAP was performed using a Leica TCS SP8 laser scanning confocal microscope. BcLOV4 was initially recruited to the membrane with a 100 ms laser pulse (λ = 405 nm). A small rectangular ROI on the membrane (∼1.5 μm × 0.5 μm; long axis parallel to the membrane) was photobleached (λ = 561 nm). The ROI was imaged at ∼60 Hz until its average fluorescence stabilized. When fit to a 1D reaction-diffusion model that accounted for membrane unbinding/rebinding of observed fluorescence recovery, the resulting D_{mem} values were below the detection limit. Therefore, the effective upper bound on D_{mem} was determined by fitting the data to a canonical model without the reaction components.[32]

Data Analysis. For functional characterization of opto-Cdc42 and opto-Tiam1, contours of cell boundaries at initial and final time points and of the DMD stimulation region were manually drawn, and then binary masks of the cell region inside (the overlap) and outside (the nonoverlap) the stimulation region were created using the Python OpenCV bitwise operation functions "and" and "xor", respectively. For opto-Cdc42 experiments, LifeAct fluorescence intensity was calculated within the overlap region, normalized to the nonoverlap region, for each time point. The change in LifeAct fluorescence was compared for BcLOV4-mCherry vs opto-Cdc42 samples, correcting for photobleaching using a nonstimulated cell in the same field of view. For opto-Tiam1 characterization, the cellular area within the overlap region was calculated at the initial and final time points. Percent change in this area was compared for BcLOV4-mCherry vs opto-Tiam1.

Statistical Analysis. For FLAG rescue quantification, each cell was treated as a separate data point, with N = 30 cells from three fields-of-view per condition, 8−12 cells per field. For functional characterization by actin polymerization and cytoskeletal dynamics, each data point was derived from one cell in an independent video, with N = 18 (opto-Cdc42) or N = 9 (opto-Tiam1) videos per condition. For opto-Tiam1 serum vs starved comparisons, N = 12 independent videos per condition were used. For opto-Cdc42 inhibitor analysis, N = 30 independent videos per condition were used. For opto-

https://doi.org/10.1021/acssynbio.1c00604
ACS Synth. Biol. 2022, 11, 515−521

Tiam1 inhibitor analysis, $N = 12$ independent videos per condition were used. Statistical significance was assessed by the two-sided nonparametric Mann−Whitney U Test, uncorrected for multiple comparisons. For time constant determination, 95% confidence intervals were calculated from exponential decay fits in MATLAB.

■ ASSOCIATED CONTENT

Supporting Information

The Supporting Information is available free of charge at https://pubs.acs.org/doi/10.1021/acssynbio.1c00604.

Instructions for domain screening primer design (readme file); 10 figures as described in the text (PDF)

■ AUTHOR INFORMATION

Corresponding Author

Brian Y. Chow − *Department of Bioengineering, University of Pennsylvania, Philadelphia, Pennsylvania 19104, United States;* orcid.org/0000-0001-6784-6404; Phone: (+1) (215) 898-5159; Email: bchow@seas.upenn.edu

Authors

Erin E. Berlew − *Department of Bioengineering, University of Pennsylvania, Philadelphia, Pennsylvania 19104, United States;* orcid.org/0000-0002-5438-6952

Keisuke Yamada − *Department of Bioengineering, University of Pennsylvania, Philadelphia, Pennsylvania 19104, United States; Department of Electrical Engineering and Bioscience, Faculty of Science and Engineering, Waseda University, Tokyo, Japan 169-8050*

Ivan A. Kuznetsov − *Department of Bioengineering, University of Pennsylvania, Philadelphia, Pennsylvania 19104, United States*

Eleanor A. Rand − *Department of Bioengineering, University of Pennsylvania, Philadelphia, Pennsylvania 19104, United States; Department of Systems Biology, Harvard University Medical School, Boston, Massachusetts 02115, United States*

Chandler C. Ochs − *Department of Bioengineering, University of Pennsylvania, Philadelphia, Pennsylvania 19104, United States; McGill University, Montreal, Quebec H3A 0G4, Canada*

Zaynab Jaber − *Structural Biology Initiative, CUNY Advanced Science Research Center, New York, New York 10031, United States; Ph.D. Program in Biochemistry, The Graduate Center, City University of New York, New York, New York 10016, United States*

Kevin H. Gardner − *Structural Biology Initiative, CUNY Advanced Science Research Center, New York, New York 10031, United States; Department of Chemistry and Biochemistry, City College of New York, New York, New York 10031, United States; Ph.D. Programs in Biochemistry, Chemistry, and Biology, The Graduate Center, City University of New York, New York, New York 10016, United States;* orcid.org/0000-0002-8671-2556

Complete contact information is available at: https://pubs.acs.org/10.1021/acssynbio.1c00604

Author Contributions

E.E.B. and K.Y. designed genetic constructs, designed experiments, conducted experiments, and analyzed data. I.A.K. constructed the patterned illumination system, conducted the FRAP measurement, and contributed to automated data analysis development. E.A.R. and C.O. assisted with genetic construct design, engineering, and assays. B.Y.C. coordinated all research. All authors contributed to data analysis and manuscript preparation.

Notes

The authors declare no competing financial interest.

■ ACKNOWLEDGMENTS

B.Y.C. acknowledges the support of National Science Foundation (NSF) Systems and Synthetic Biology (MCB 1652003), NIH/National Institute on Drug Abuse (R21 DA040434), and NIH/National Institute of Neurological Disorders and Stroke (NINDS) (R01 NS101106). E.E.B. acknowledges the fellowship support of the National Institute of Neurological Disorders and Stroke of the National Institutes of Health (T32 NS091006). I.A.K. acknowledges the fellowship support of the Paul and Daisy Soros Fellowship for New Americans and the NIH/National Institute of Mental Health F30 Award. K.H.G. acknowledges support from the NIH/National Institute of General Medical Sciences (R01 GM106239).

■ REFERENCES

(1) Harper, S. M.; Neil, L. C.; Gardner, K. H. Structural basis of a phototropin light switch. *Science* **2003**, *301* (5639), 1541−4.

(2) Wu, Y. I.; Frey, D.; Lungu, O. I.; Jaehrig, A.; Schlichting, I.; Kuhlman, B.; Hahn, K. M. A genetically encoded photoactivatable Rac controls the motility of living cells. *Nature* **2009**, *461* (7260), 104−8.

(3) He, L.; Jing, J.; Zhu, L.; Tan, P.; Ma, G.; Zhang, Q.; Nguyen, N. T.; Wang, J.; Zhou, Y.; Huang, Y. Optical control of membrane tethering and interorganellar communication at nanoscales. *Chem. Sci.* **2017**, *8* (8), 5275−5281.

(4) Natwick, D. E.; Collins, S. R. Optimized iLID Membrane Anchors for Local Optogenetic Protein Recruitment. *ACS Synth. Biol.* **2021**, *10* (5), 1009−1023.

(5) Ma, G.; He, L.; Liu, S.; Xie, J.; Huang, Z.; Jing, J.; Lee, Y. T.; Wang, R.; Luo, H.; Han, W.; Huang, Y.; Zhou, Y. Optogenetic engineering to probe the molecular choreography of STIM1-mediated cell signaling. *Nat. Commun.* **2020**, *11* (1), 1039.

(6) Hannanta-Anan, P.; Glantz, S. T.; Chow, B. Y. Optically inducible membrane recruitment and signaling systems. *Curr. Opin Struct Biol.* **2019**, *57*, 84−92.

(7) Berlew, E. E.; Kuznetsov, I. A.; Yamada, K.; Bugaj, L. J.; Chow, B. Y. Optogenetic Rac1 engineered from membrane lipid-binding RGS-LOV for inducible lamellipodia formation. *Photochem. Photobiol. Sci.* **2020**, *19*, 353.

(8) Berlew, E. E.; Kuznetsov, I. A.; Yamada, K.; Bugaj, L. J.; Boerckel, J. D.; Chow, B. Y. Single-Component Optogenetic Tools for Inducible RhoA GTPase Signaling. *Adv. Biol. (Weinh)* **2021**, *5*, e2100810.

(9) Glantz, S. T.; Carpenter, E. J.; Melkonian, M.; Gardner, K. H.; Boyden, E. S.; Wong, G. K.; Chow, B. Y. Functional and topological diversity of LOV domain photoreceptors. *Proc. Natl. Acad. Sci. U. S. A.* **2016**, *113* (11), E1442−51.

(10) Glantz, S. T.; Berlew, E. E.; Jaber, Z.; Schuster, B. S.; Gardner, K. H.; Chow, B. Y. Directly light-regulated binding of RGS-LOV photoreceptors to anionic membrane phospholipids. *Proc. Natl. Acad. Sci. U. S. A.* **2018**, *115* (33), E7720−E7727.

(11) Chrzanowska-Wodnicka, M.; Burridge, K. Rho-stimulated contractility drives the formation of stress fibers and focal adhesions. *J. Cell Biol.* **1996**, *133* (6), 1403−15.

(12) Etienne-Manneville, S.; Hall, A. Rho GTPases in cell biology. *Nature* **2002**, *420* (6916), 629−35.

(13) Sit, S. T.; Manser, E. Rho GTPases and their role in organizing the actin cytoskeleton. *J. Cell Sci.* **2011**, *124*, 679−83.
(14) Heasman, S. J.; Ridley, A. J. Mammalian Rho GTPases: new insights into their functions from in vivo studies. *Nat. Rev. Mol. Cell Biol.* **2008**, *9* (9), 690−701.
(15) Bos, J. L.; Rehmann, H.; Wittinghofer, A. GEFs and GAPs: critical elements in the control of small G proteins. *Cell* **2007**, *129* (5), 865−77.
(16) Lamas, I.; Weber, N.; Martin, S. G. Activation of Cdc42 GTPase upon CRY2-Induced Cortical Recruitment Is Antagonized by GAPs in Fission Yeast. *Cells* **2020**, *9* (9), 2089.
(17) Lamas, I.; Merlini, L.; Vjestica, A.; Vincenzetti, V.; Martin, S. G. Optogenetics reveals Cdc42 local activation by scaffold-mediated positive feedback and Ras GTPase. *PLoS Biol.* **2020**, *18* (1), e3000600.
(18) Das, S.; Yin, T.; Yang, Q.; Zhang, J.; Wu, Y. I.; Yu, J. Single-molecule tracking of small GTPase Rac1 uncovers spatial regulation of membrane translocation and mechanism for polarized signaling. *Proc. Natl. Acad. Sci. U. S. A.* **2015**, *112* (3), E267−76.
(19) Michiels, F.; Habets, G. G.; Stam, J. C.; van der Kammen, R. A.; Collard, J. G. A role for Rac in Tiam1-induced membrane ruffling and invasion. *Nature* **1995**, *375* (6529), 338−40.
(20) Michiels, F.; Stam, J. C.; Hordijk, P. L.; Kammen, R. A. v. d.; Stalle, L. R.-V.; Feltkamp, C. A.; Collard, J. G. Regulated membrane localization of Tiam1, mediated by the NH2-terminal pleckstrin homology domain, is required for Rac-dependent membrane ruffling and C-Jun NH2-terminal kinase activation. *J. Cell Biol.* **1997**, *137* (2), 387−98.
(21) Wells, C. M.; Walmsley, M.; Ooi, S.; Tybulewicz, V.; Ridley, A. J. Rac1-deficient macrophages exhibit defects in cell spreading and membrane ruffling but not migration. *J. Cell Sci.* **2004**, *117* (Pt 7), 1259−68.
(22) Guntas, G.; Hallett, R. A.; Zimmerman, S. P.; Williams, T.; Yumerefendi, H.; Bear, J. E.; Kuhlman, B. Engineering an improved light-induced dimer (iLID) for controlling the localization and activity of signaling proteins. *Proc. Natl. Acad. Sci. U. S. A.* **2015**, *112* (1), 112−7.
(23) Ridley, A. J.; Hall, A. The small GTP-binding protein rho regulates the assembly of focal adhesions and actin stress fibers in response to growth factors. *Cell* **1992**, *70* (3), 389−399.
(24) Ren, X. D.; Kiosses, W. B.; Schwartz, M. A. Regulation of the small GTP-binding protein Rho by cell adhesion and the cytoskeleton. *EMBO J.* **1999**, *18* (3), 578−85.
(25) Borm, B.; Requardt, R. P.; Herzog, V.; Kirfel, G. Membrane ruffles in cell migration: indicators of inefficient lamellipodia adhesion and compartments of actin filament reorganization. *Exp. Cell Res.* **2005**, *302* (1), 83−95.
(26) Valon, L.; Etoc, F.; Remorino, A.; di Pietro, F.; Morin, X.; Dahan, M.; Coppey, M. Predictive Spatiotemporal Manipulation of Signaling Perturbations Using Optogenetics. *Biophys. J.* **2015**, *109* (9), 1785−97.
(27) Van Geel, O.; Hartsuiker, R.; Gadella, T. W. J. Increasing spatial resolution of photoregulated GTPases through immobilized peripheral membrane proteins. *Small GTPases* **2020**, *11* (6), 441−450.
(28) Machacek, M.; Hodgson, L.; Welch, C.; Elliott, H.; Pertz, O.; Nalbant, P.; Abell, A.; Johnson, G. L.; Hahn, K. M.; Danuser, G. Coordination of Rho GTPase activities during cell protrusion. *Nature* **2009**, *461* (7260), 99−103.
(29) Byrne, K. M.; Monsefi, N.; Dawson, J. C.; Degasperi, A.; Bukowski-Wills, J. C.; Volinsky, N.; Dobrzynski, M.; Birtwistle, M. R.; Tsyganov, M. A.; Kiyatkin, A.; Kida, K.; Finch, A. J.; Carragher, N. O.; Kolch, W.; Nguyen, L. K.; von Kriegsheim, A.; Kholodenko, B. N. Bistability in the Rac1, PAK, and RhoA Signaling Network Drives Actin Cytoskeleton Dynamics and Cell Motility Switches. *Cell Syst* **2016**, *2* (1), 38−48.
(30) Bagci, H.; Sriskandarajah, N.; Robert, A.; Boulais, J.; Elkholi, I. E.; Tran, V.; Lin, Z. Y.; Thibault, M. P.; Dube, N.; Faubert, D.; Hipfner, D. R.; Gingras, A. C.; Cote, J. F. Mapping the proximity interaction network of the Rho-family GTPases reveals signalling pathways and regulatory mechanisms. *Nat. Cell Biol.* **2020**, *22* (1), 120−134.
(31) Berlew, E. E.; Kuznetsov, I. A.; Yamada, K.; Bugaj, L. J.; Boerckel, J. D.; Chow, B. Y. Single-component optogenetic tools for inducible RhoA GTPase signaling. *bioRxiv* **2021**, *5*, 2100810.
(32) Ellenberg, J.; Siggia, E. D.; Moreira, J. E.; Smith, C. L.; Presley, J. F.; Worman, H. J.; Lippincott-Schwartz, J. Nuclear membrane dynamics and reassembly in living cells: targeting of an inner nuclear membrane protein in interphase and mitosis. *J. Cell Biol.* **1997**, *138* (6), 1193−206.

https://doi.org/10.1021/acssynbio.1c00604
ACS Synth. Biol. 2022, 11, 515−521